LANGMUIR

pubs.acs.org/Langmuir Article

Antioxidant Hydrogen-Atom-Transfer to DPPH Radicals by Hybrids of {Hyaluronic-Acid Components}@SiO_2

Annita Theofanous, Irene Sarli, Fotini Fragou, Eleni Bletsa, Yiannis Deligiannakis, and Maria Louloudi*

Cite This: *Langmuir* 2022, 38, 12333−12345 Read Online

ACCESS | Metrics & More | Article Recommendations | Supporting Information

ABSTRACT: Hydrogen-atom-transfer (HAT) is among the key mechanisms of antioxidant and antiradical activity in natural systems. Hyaluronic acid (HyA) is currently used extensively in health and cosmetics applications. Herein it is shown that {HyA@SiO_2} hybrids based on hyaluronic acid (HyA) components grafted on SiO_2 nanoparticles enable significant HAT activity versus DPPH radicals, while the homogeneous HyA counterparts are practically inactive. The {HyA@SiO_2} hybrids consist of the two building blocks of HyA [D-glucuronic acid (GLA) and N-acetyl-D-glucosamine (GLAM)] covalently grafted on SiO_2 nanoparticles. Based on the kinetic-thermodynamic Arrhenius study, we show that the {SiO_2@GLA} hybrids operate spontaneously via hydrogen-atom-transfer (HAT) with a low activation energy barrier, i.e., by $\Delta E_a \sim 20$ kJ/mol vs the nongrafted counterparts. Moreover, a doubly grafted {GLA@SiO_2@GLAM} nanohybrid, i.e. that contains both components of HyA, shows the most significant antioxidant activity. FTIR and Raman analysis reveal that local H-bonding between the SiO_2 matrix, GLA, and GLAM in {GLA@SiO_2@GLAM} decreases the activation barrier of the HAT mechanism. Thus, {GLA@SiO_2@GLAM} nanohybrids exemplify a novel family of materials that are not the mere sum of their components. The present case is the first example of non-phenolic molecules being able to perform antiradical HAT, opening new perspectives not foreseen until today.

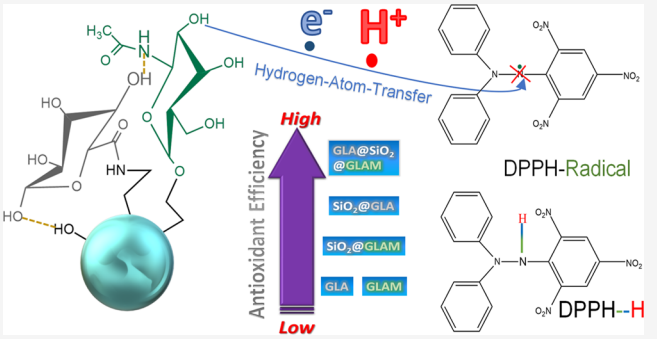

1. INTRODUCTION

Antioxidants are radical-abating moieties that attract intense scientific and economic interest in research and industry related to human health,[1,2] food,[3] and polymers,[4] to name a few. They are unequivocally beneficial in improving life quality since they can prevent or postpone the onset of degenerative diseases.[1] Antiradical-antioxidants at low concentrations delay (or prevent) the deterioration of cells, or molecules, by adverse radical reactions or radical-related oxidation;[5−7] thus, they can protect the human body against damage by reactive oxygen species (ROS).[1] Organic compounds, e.g., ascorbates, tocopherols, flavonoids, carotenoids, and phenolic acids,[1] that bear at least one functional group that participates in an antioxidant mechanism without undergoing significant alteration of its molecular structure, are well-known natural antioxidants.

Among the most efficient natural antioxidants, polyphenols successfully neutralize free radicals via their -OH groups.[8] It has been widely established that the key event in the antioxidant activity of polyphenols is hydrogen-atom-transfer (HAT),[9,10] i.e. a *concomitant* transfer of one proton (H^+) and one electron (e^-) as an (H^+/e^-) pair. There is a well-established correlation between phenolic content and the total antioxidant activity of various plant extracts.[11,12] DPPH (2,2-diphenyl-1-picrylhydrazyl) is a stable radical that is used as a reference to evaluate the HAT process for antioxidants.[13−15] As clarified in the critical review of Foti et al., the DPPH assay is more appropriate for assessing the HAT process in aprotic solvents.[16]

Recently, we have demonstrated that DPPH can be a credible probe of the HAT process in hybrid antioxidant materials, e.g. gallic-acid@SiO_2[17,18] or more complex {polyphenol-polymer@SiO_2}[19] in methanol. More generally, for the study of HAT to DPPH, a proper kinetic-thermodynamic study can provide detailed information on the number of transferred (H^+/e^-) hydrogen atoms and the activation barriers.[10]

Hyaluronic acid (HyA) is a naturally occurring biodegradable polymer that has found many applications in medicine in the recent decade.[20] The chemical structure of HyA consists of two repeating units: [D-glucuronic acid] and [N-acetyl-D-glucosamine].[21] HyA is a linear, unbranched polysaccharide

Received: July 28, 2022
Revised: September 12, 2022
Published: September 27, 2022

https://doi.org/10.1021/acs.langmuir.2c02021
Langmuir 2022, 38, 12333−12345

Scheme 1. (A) Synthesis and Structural Depiction of {SiO_2@GLA}, {SiO_2@GLAM}, and the Doubly Grafted {GLA@SiO_2@GLAM} Nanohybrids, and (B) Molecular Structure of the Two Building Blocks of Hyaluronic Acid Containing Repeating Units of D-Glucuronic Acid and N-Acetyl-D-Glucosamine

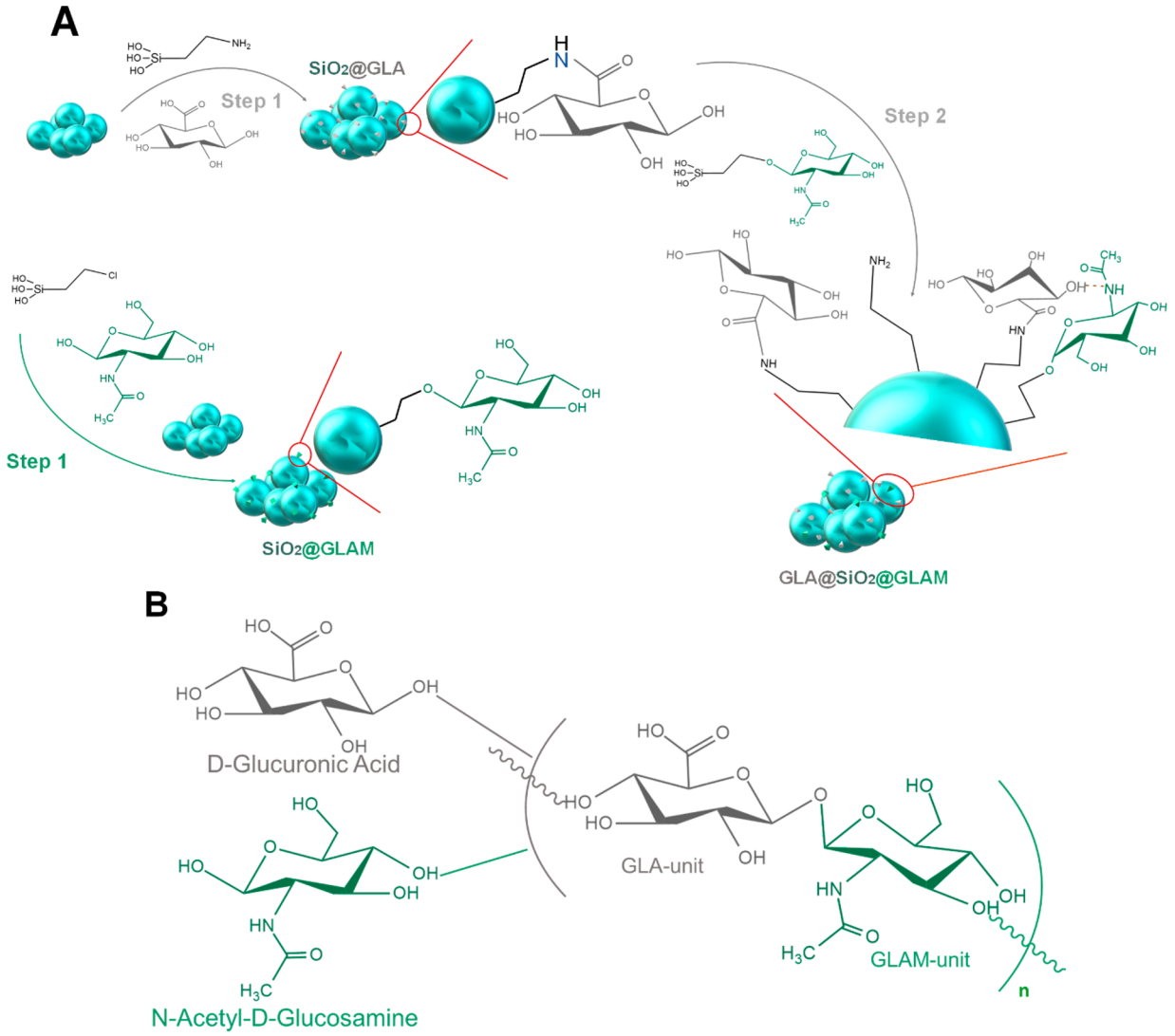

consisting of repeated disaccharide units. It has a ubiquitous distribution throughout the human body and is involved in a wide range of bioprocesses.[22] In brief, HyA is a significant component of the extracellular matrix.[23] Cells in the human body can synthesize HyA at some stages of their cell cycle, implicating its function in fundamental biological processes.[24] The chemical and physical properties of HyA define its versatile properties, such as its outstanding biocompatibility, nonimmunogenicity, biodegradability, and viscoelasticity. As such, HyA is an ideal biomaterial for cosmetics, medical, and pharmaceutical applications.[20] Herein, we provide the first proof that components of HyA can have significant antioxidant activity if properly grafted on a SiO_2 surface. At the same time, the present research provides thermodynamic evidence of the factors which determine the antioxidant activity of HyA components.

During the past decade, incorporating natural antioxidants in material matrices has been exploited as an advanced technology to overcome the drawbacks of natural antioxidants such as autodeactivation via radical polymerization and nonoptimal radical scavenging energetics, etc. Pertinent examples include grafting of gallic acid (GA) on organic supports such as chitosan[25−27] and gelatin[28] and of caffeic acid on chitosan[29] and polypropylene.[30] As we have demonstrated, in a more general context, appropriate inorganic materials/particles can be utilized as support materials for engineering efficient {antioxidant-inorganic} nanohybrids. For example, a commercial montmorillonite clay, laponite, can be used to stabilize tyrosine-based[31] and gallic acid-based[17] phenolic radicals via intercalation[31,32] in the interlayer space of the clay. Moreover, more complex polyphenols such as humic acids grafted covalently on silica gel exhibit enhanced antioxidant activity.[32] Other works demonstrate that an appropriate solid support can provide critical advantages regarding the stability and performance of phenolic antioxidants.[17,19,33] This has been amply exemplified in the case of gallic acid immobilized on SiO_2 nanoparticles, where the nanohybrid {GA-SiO_2} showed maximum hydrogen-atom-transfer capacity, i.e., 2 hydrogens atoms per GA molecule,[17] and zero deactivation, due to prevention of adverse radical−radical coupling between GA molecules.[33] A detailed thermodynamic analysis revealed that the surface-anchored

https://doi.org/10.1021/acs.langmuir.2c02021
Langmuir 2022, 38, 12333−12345

GA phenolics might show enhanced antioxidant efficiency due to H-bonding between adjacent OH moieties.[17,33]

This work introduces a novel family of hybrid nano-antioxidants based on the building blocks of HyA, i.e., D-glucuronic acid (herein code-named GLA) and N-acetyl-D-glucosamine (herein code-named GLAM), covalently grafted on the surface of SiO_2 (see Scheme 1). A synthetic protocol for the development of efficient antioxidant hybrids has been established. Utilizing the advantages of the SiO_2 supporting material, it is possible to control the interfacial processes.

The strategic hypothesis of this work was that, although GLA or GLAM monomers show poor antioxidant activity in solution, this changes when assembled on SiO_2.[19,33] Thus, if appropriately grafted on the SiO_2 surface, under a controlled interfacial process, the {SiO_2@GLA} or {SiO_2@GLAM} nanohybrids can be optimized toward having antioxidant activity. Interestingly, we found that the "doubly grafted" {GLA@SiO_2@GLAM} hybrid shows enhanced antioxidant activity. Detailed spectroscopic, kinetic, and thermodynamic experiments were performed to assess the radical scavenging capacity (RSC) of the hybrids to understand the physicochemical basis of this novel phenomenon. For this purpose, nanohybrid materials comprising {SiO_2@GLA}, {SiO_2@GLAM}, as well as doubly grafted {GLA@SiO_2@GLAM} hybrids have been synthesized. As a reference nanomaterial, {SiO_2@GA} NPs have also been analyzed, whose antioxidant properties are well understood.[33]

The specific aims of the present work were: [a] to develop efficient nanohybrid antioxidants based on hyaluronic-acid components, with emphasis on the doubly grafted nanohybrid, [b] to experimentally study the interfacial hydrogen-atom-transfer antioxidant efficiency, and [c] to analyze the interfacial HAT effects in the context of thermodynamics related to the nanointerface.

2. MATERIALS AND METHODS

2.1. Chemicals and SiO_2 NPs. 3-aminopropyl-triethoxysilane (APTES, >99%), D-glucuronic acid (GLA, >99%), N-acetyl-D-glucosamine (GLAM, >99%), (3-chloropropyl) trimethoxysilane (>97%), and N-(3-(dimethylamino)propyl)-N′-ethylcarbodiimide hydrochloride (EDC, >98%) were obtained from Sigma-Aldrich. Solvents: Acetone (purity >99.8%), ethanol (purity >99.9%), methanol (purity >99.9%), and toluene (purity >99.5%) were from Merck. Silica gel 60 (0.040−0.063 mm) for column chromatography was obtained from Merck. 2,2-Diphenyl-1-picrylhydrazyl (DPPH) was obtained from Sigma-Aldrich.

2.2. Synthesis of {SiO_2@GLA}: Immobilization of D-Glucuronic Acid. Silica was dried at 140 °C for 24 h. Aminopropyl-SiO_2 (APTES-SiO_2) was prepared with 5 g of dry silica gel reacting with 5 mL of (3-aminopropyl)triethoxysilane (APTES) in 50 mL of toluene. The solution was refluxed for 24 h at 80 °C, then rinsed three times with toluene, three times with ethanol, and three times with acetone, and dried for 24 h in a drying pistol at 80 °C. The obtained particles were {aminopropyl-SiO_2}, herein named SiO_2@NH_2 for brevity (Scheme S1 in the Supporting Information file). One gram of SiO_2@NH_2 was dispersed in 50 mL of toluene, and then GLA and EDC were added to the suspension. Covalent immobilization of D-glucuronic acid (GLA) on SiO_2@NH_2 was achieved via the formation of amide bonds between the amine groups of SiO_2@NH_2 and the carboxyl group of GLA activated by the EDC coupler. A (GLA:EDC) mass ratio (3:1) was used, e.g., 300 mg of GLA and 100 mg of EDC per gram of SiO_2@NH_2. The mixture was refluxed for 24 h at 80 °C. The solution was then centrifuged at a ROTINA Hettich 6000 rpm for 15 min at 25 °C, rinsed three times with toluene, three times with ethanol, and three times with acetone, and dried at 80 °C for 24 h. The chemical reactions are analytically described in Scheme S1 in the Supporting Information file.

2.3. Synthesis of {SiO_2@GLAM}: Immobilization of N-Acetyl-D-Glucosamine. SiO_2@GLAM particles were prepared with 0.40 g of N-acetyl-D-glucosamine reacting with 273 μL of 3-chloropropyl-trimethoxysilane in 10 mL of methanol (MeOH). The mixture was refluxed for 48 h at 60 °C. Then, 1 g of dry SiO_2 and 5 mL of ethanol (EtOH) were added. The mixture was refluxed for 24 h at 60 °C. Then, the solution was centrifuged in a ROTINA Hettich, 6000 rpm, for 15 min at room temperature (RT) and rinsed three times with methanol and three times with ethanol and dried at 60 °C for 24 h (see Scheme S2 in the Supporting Information file for analytical chemical reactions).

2.4. Synthesis of the Doubly Grafted {GLA@SiO_2@GLAM} Hybrid. The {GLA@SiO_2@GLAM} hybrid with molecular ratio {GLA:GLAM} equal to [2:1] was prepared by the reaction of 0.2046 g of N-acetyl-D-glucosamine with 137 μL of 3-chloropropyl-trimethoxysilane in 7 mL of methanol (MeOH). The mixture was refluxed for 48 h at 60 °C. After 48 h, 0.5024 g of dry SiO_2@GLA and 4.5 mL of ethanol (EtOH) were added. The mixture was refluxed for 24 h at 60 °C. Then the solution was centrifuged for 15 min at room temperature (RT), rinsed three times with methanol and ethanol, and dried at 60 °C for 24 h (see Scheme S3 in the Supporting Information file, where all the reactions that take place are described). The protocol for the preparation of the doubly grafted {GLA@SiO_2@GLAM} nanohybrid with molecular ratio {GLA:GLAM} equal to [3:1] is given in the Supporting Information (Section 2.4), and for the reactions, see Scheme S4 in the Supporting Information file.

2.5. Instrumentation. *2.5.1. TEM Microscopy.* The nanomaterial morphology was analyzed by high-resolution transmission electron microscopy (HRTEM) using a Philips CM 20 microscope operated at 200 kV and provided 0.25 nm resolution. Before measurements, the samples were mildly ground in a mortar and dry loaded onto a support film (Lacey Carbon, 300 mesh (Cu)). Recorded pictures were analyzed by Gatan Digital Micrograph software.

2.5.2. Thermogravimetric Analysis (TG-TDA). The organic loading in nanohybrid particles was measured by thermogravimetric (TGA) analysis performed using a DTG-60 instrument (SHIMADZU) and the analyzer TA-60 WS (SHIMADZU). In all measurements, approximately 10 mg of material was used and placed in a platinum capsule on one arm of the thermocouple. An empty platinum capsule was also used as a reference in the other arm. Finally, the measurements were made at a temperature range of 20 to 700 °C, at a rate of 10 °C·min^{-1}, under synthetic air flow.

2.5.3. Raman Spectra. Raman spectra were recorded with a HORIBA-Xplora Plus instrument coupled to an Olympus BX41 microscope, equipped with a 785 nm diode laser as an excitation source. The spectra were recorded for 10 s with 30 accumulations to obtain a good signal-to-noise ratio.

2.5.4. Fourier Transformed Infrared Spectroscopy (FT-IR). FT-IR measurements were performed in KBr pellets using a Nicolet TM IS-5TM FT-IR spectrometer. The powder mixture was molded and compressed uniaxially (10N) with a hydraulic press to create a compressed tablet with a diameter of 1 cm and a height of 1−15 mm. The final spectra are the average of 32 spectra, measured in the range of 400−4000 cm^{-1} with a distinctive ability of 2 cm^{-1}.

2.5.5. Specific Surface Areas (SSAs). The samples' specific surface areas (SSAs) were determined from N_2 adsorption/desorption isotherms. The N_2 adsorption/desorption isotherms were measured at 77 K on a Quantachrome NOVAtouch LX2 instrument. Before the measurements, the samples were degassed at 150 °C for 16 h under a vacuum. The surface area (SSA) was determined using the Brunauer−Emmett−Teller (BET) method for adsorption and desorption data points. The specific surface area (SBET) was found using adsorption data points in the relative pressure P/P_o range of 0.1−0.3. While the Barrett−Joyner−Halenda (BJH) method was used for the pore radius using the absorption data points from 0.35 to 0.99 P/P_o, and the total pore volume was obtained at the 0.99 P/P_o points.

2.5.6. Low-Temperature UV−Vis Spectroscopy. A low-temperature UV−vis spectrophotometer Hitachi U-2900 instrument was

https://doi.org/10.1021/acs.langmuir.2c02021
Langmuir 2022, 38, 12333−12345

equipped with a Unisoku cryostat, inserted inside the UV−vis spectrophotometer beam chamber. This system allows digital control of sample temperature in the range of +100 °C to −100 °C within ±0.1 °C. Cooling of the sample was achieved by a controlled flow of cold N_2 gas derived from the heating of liquid N_2. Herein, for the Arrhenius analysis, the nanohybrid materials' kinetics were recorded at different temperatures of −15 °C, 0 °C, +15 °C, and +25 °C, and these kinetics data were used to calculate the activation energy E_a.

2.6. Evaluation of the Antioxidant Radical Scavenging Capacity (RSC). Evaluation of the radical scavenging capacity of all hybrid nanoparticles was performed using the DPPH method,[15,17,18,34] which offers a suitable basis for comparative evaluation of the RSC for most natural antioxidants,[15,27,35] as well as functionalized polymers.[25,26,28] The particles were dispersed by adding 5 mg in 5 mL of methanol (MeOH) and sonicated using a cup-horn sonicator (Sonic-VCX-500) at a power of 100 W for 10 min in cycles of 1-s power on/off (overall 0.5 kJ for 5 mL). The kinetics of DPPH-radical scavenging was monitored by recording the decay of the UV−visible spectrum of DPPH[17] at different temperature experiments.[17−19]

At each kinetic experiment, 500 μL of DPPH solution in MeOH (30×10^{-6} mol·L^{-1}) was added in situ in a standard quartz cuvette, 1 × 1 × 3 cm, 3 mL volume (Hellma Suprasil quartz glass, 100-OS), under stirring. A dilute particle suspension of (360 mg·L^{-1}) in MeOH was used to allow measurements nonperturbed by particle dispersion opacity. The absorbance intensity at 515 nm (I_{515}) was used to quantify the concentration of DPPH radicals in MeOH solution according to the standard method established by Brand-Williams.[15] The freshly prepared DPPH/MeOH solution of 30 μM concentration resulted in I_{515} = 0.32.[17] Kinetic measurements were run immediately after adding DPPH and repeated at least twice for each material.

In this type of DPPH radical quenching, the initial phase in the kinetic curve corresponds to a hydrogen-atom-transfer (HAT) process.[17] Accordingly, kinetic analysis was done for different temperatures, using the Arrhenius equation (eq 1)[36] as follows: using the kinetic rate values (k) vs T, the Arrhenius plot {ln k vs $[1(T \times 1000)^{-1}]$} was constructed. Using the Arrhenius equation (eq 1), the activation energy barrier, E_a, was estimated from the slope of the plot.[31]

$$\ln k = -\frac{E_\alpha}{RT} + \ln A \tag{1}$$

A is the pre-exponential factor determined as the offset of the {ln k vs $[1(T \times 1000)^{-1}]$} plot. Two kinetic phases were distinguished in certain materials, i.e., in the doubly grafted {GLA@SiO_2@GLAM} nanohybrid. These could be fitted by two Arrhenius components; see eq 2.

$$\ln k = \left[-\frac{E_{\alpha 1}}{RT} + \ln A_1\right] + \left[-\frac{E_{\alpha 2}}{RT} + \ln A_2\right] \tag{2}$$

The two components correspond to two distinct HAT activities with different activation barriers, E_{a1} and E_{a2}.

3. RESULTS AND DISCUSSION

3.1. Characterization of SiO_2@GLA, SiO_2@GLAM, and {GLA@SiO_2@GLAM}. *3.1.1. Morphology of the Materials.* The surface functionalization of SiO_2 NPs, as evidenced by color changes of the white pristine SiO_2 particles, to brown, faint-yellow, and faint-brown, is presented in Figure 1. The BET data (Figure 1) show that grafting decreases the specific surface area by ∼25%, accompanied by a narrowing of the pore dimensions; for more details, see Figure S1 in the Supporting Information file and Table 1. The TEM images of SiO_2, functionalized SiO_2@GLA, and functionalized {GLA@SiO_2@GLAM} hybrids are depicted in the top row of Figure 1. The SiO_2 supporting nanomaterial (Figure 1, upper left) is composed of spherical particles that combine to form chain-like agglomerates. After the modification, the surface becomes more compact since the monosaccharides fill the available pores.

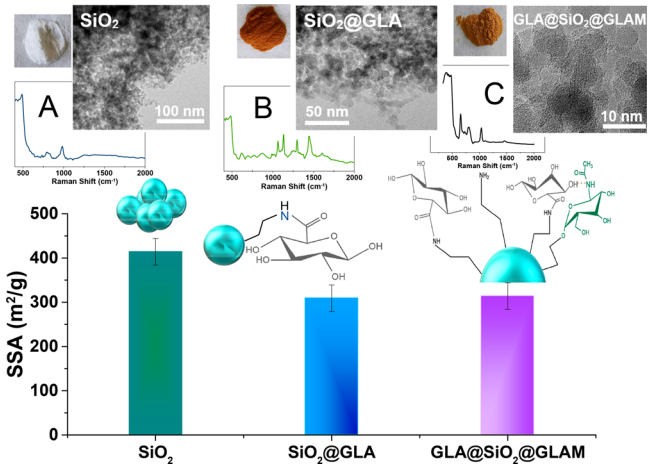

Figure 1. *(Upper row)* TEM images and Raman spectra and *(lower row)* specific surface areas (m^2 g^{-1}) of (A) pure SiO_2, (B) functionalized SiO_2@GLA NPs, and (C) functionalized {GLA@SiO_2@GLAM} NPs.

3.1.2. Thermogravimetric Analysis. The thermogravimetric analysis of nanohybrid doubly grafted {GLA@SiO_2@GLAM} with a molecular ratio of [GLA:GLAM] equal to [2:1] is given in Figure 2 for a more comprehensive analysis of the surface-grafting process. The TGA analysis of {GLA@SiO_2@GLAM} with a molecular ratio of [GLA:GLAM] equal to [3:1] is presented in Figure S2 in the Supporting Information file; for a more detailed analysis, see Section.3.1.2 in the Supporting Information file. For the hybrid {GLA@SiO_2@GLAM} (Figure 2), we see that the gradual mass loss corresponds to 16.4% of the modified material. First, we evaluate the total mass loss of SiO_2@NH_2 using the TGA data in Figure 2(A). The total mass loss rate for 150−550 °C is 5.3%, corresponding to 0.91 mmol of $NH_2(CH_2)_3$ per gram of hybrid nanomaterial, based mainly on the exothermic curve in the range 250−350 °C. In the second stage of synthesis, we have the production of the SiO_2@GLA nanohybrid, where the gradual loss of mass [(blue line) in Figure 2(B)] is completed by a 12.3% percentage, assigned to the combustion of grafted organics. Since this nanomaterial has already been modified with the $NH_2(CH_2)_3$ group, the percentage of 5.3% corresponding to the SiO_2@NH_2 is subtracted, leaving a 7.0% corresponding to 0.29 mmol GLA/g. Finally, a 16.4% loss of mass for the final nanohybrid doubly grafted {GLA@SiO_2@GLAM} was observed [Figure 2(C) (blue line)]. 12.3% corresponding to the $NH_2(CH_2)_3$ and GLA groups is deducted, and the calculations for GLAM are made on 4.1%, corresponding to 0.15 mmol GLAM/g of the modified material. TGA analysis (analyzed below) shows a significant amount of grafted organic on the SiO_2 surface that approaches ∼29% w/w in the doubly grafted {GLA@SiO_2@GLAM} 3:1. This, together with the SSA data, indicates an extensive, complete coverage of the SiO_2 particle surface by the grafted organics, especially in the doubly grafted {GLA@SiO_2@GLAM} nanohybrids (see Table 1).

3.1.3. Vibrational Spectroscopy (FTIR and Raman). 3.1.3.1. FT-IR Spectroscopy. Figure 3 shows the FTIR spectra of the hybrid materials, SiO_2@GLA, SiO_2@GLAM, and doubly grafted {GLA@SiO_2@GLAM}, in comparison to nonfunction-

https://doi.org/10.1021/acs.langmuir.2c02021
Langmuir 2022, 38, 12333−12345

Table 1. Chemical and Physical Characteristics of the Present SiO_2-Based Nanohybrids

Material	*Organic loading (%)*	*SSA($m^2 \cdot g^{-1}$)*	*Average Pore Volume($cc \cdot g^{-1}$)*	*Pore radius Dv(r) (nm)*
SiO_2		414 ± 1	0.73 ± 0.005	3.2 ± 0.05
SiO_2@GLA	12.9 ± 0.5	309 ± 1	0.47 ± 0.005	2.4 ± 0.05
SiO_2@GLAM	14.6 ± 0.5	311 ± 1	0.44 ± 0.005	2.3 ± 0.05
{GLA@SiO_2@GLAM} 2:1	16.4 ± 0.5	314 ± 1	0.42 ± 0.005	2.1 ± 0.05
{GLA@SiO_2@GLAM} 3:1	29.2 ± 0.5	318 ± 1	0.41 ± 0.005	2.1 ± 0.05

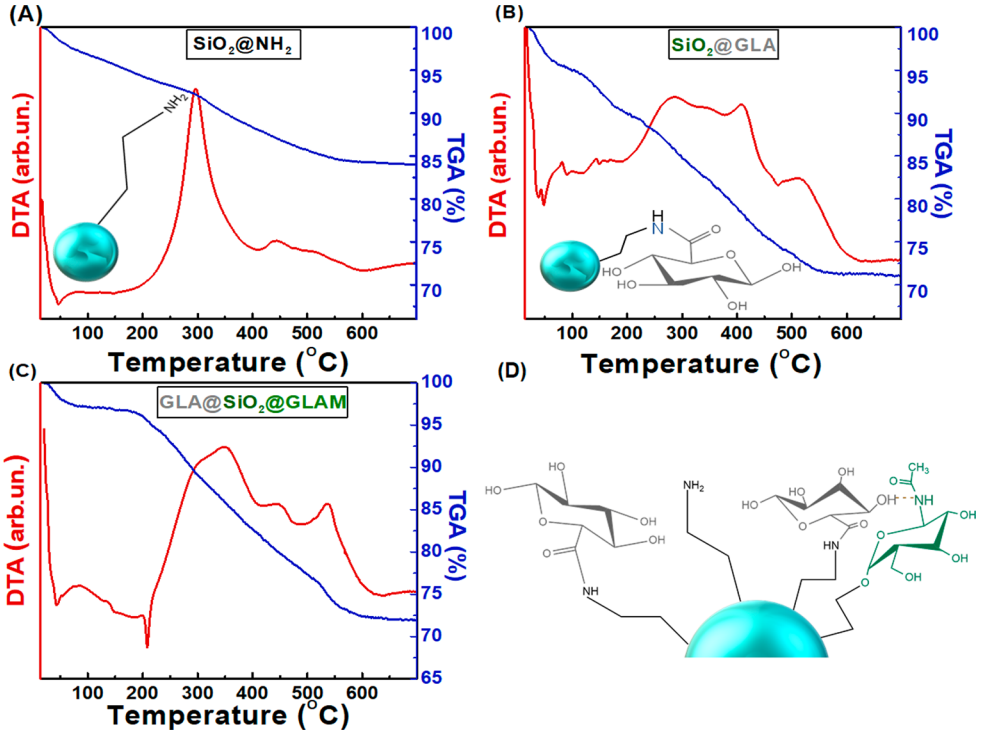

Figure 2. Thermogravimetric analysis of (A) SiO_2@NH_2, (B) nanohybrid material SiO_2@GLA, (C) nanohybrid doubly grafted {GLA@SiO_2@GLAM} [2:1], and (D) molecular structure of the nanohybrid doubly grafted {GLA@SiO_2@GLAM} [2:1].

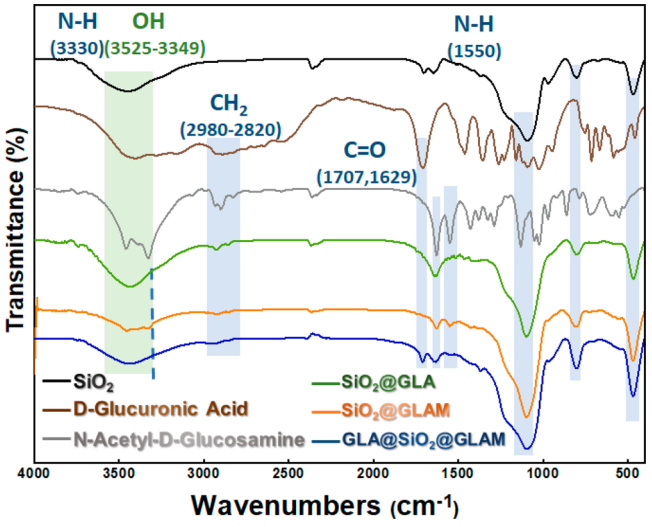

Figure 3. FT-IR spectra of SiO_2 (black line), D-glucuronic acid (GLA) (brown line), N-acetyl-D-glucosamine (GLAM) (gray line), SiO_2@GLA (green line), SiO_2@GLAM (orange line), and the doubly grafted hybrid {GLA@SiO_2@GLAM} [2:1] (blue line).

alized SiO_2 and powders of D-glucuronic acid and N-acetyl-D-glucosamine. In Figure 3 (black line), the SiO_2 is characterized by the 467, 801, and 1096 cm^{-1} peaks, which can be attributed to the swing vibrations (R), symmetric stretching vibrations (SS), and asymmetric stretching vibrations (AS), of the Si−O−Si bond of silicon mesh, respectively (Figure S3 in the Supporting Information file).[37,38]

In Figure 3 (green line), the FTIR spectra of D-glucuronic acid are characterized by the sharp 3407, 3280, and 3160 cm^{-1} peaks assigned to the OH groups of D-glucuronic acid.[39] The peaks at 2895 and 2931 cm^{-1} are attributed to the $\nu(CH_2)$ vibrations, while the peak at 1707 cm^{-1} corresponds to the bending vibrations of the $\delta(C{=}O)$ bond.[39] The 1460, 1358, 1263, and 1224 cm^{-1} peaks are due to the $\nu(CH_2)$.[39] The peak at 1163 cm^{-1} is due to the presence of the C—O group; see the molecular structure in Scheme 1 and Figure S3(A, C) in the Supporting Information file.

Figure 3 (gray line) presents the FTIR spectrum of N-acetyl-D-glucosamine. The 3461 and 3316 cm^{-1} peaks in this spectrum are assigned to OH groups of N-acetyl-D-glucosamine. The 1287, 1333, 1372, 1433, 2826, 2911, and 2935 cm^{-1} peaks are assigned to the $\nu(CH_2)$ vibrations.[39] Also, the 1629 cm^{-1} peak is due to the $\nu(C{=}O)$ vibrations of the carboxyl groups of N-acetyl-D-glucosamine. The peak at 1550 cm^{-1} is assigned to the N—H bond vibrations[39] (Figure S3(B, C) in the Supporting Information file).

In Figure 3 (green line), the FTIR spectrum of SiO_2@GLA is characterized by a broad peak from 3349 to 3525 cm^{-1}, which is assigned to the OH groups, while the vibrations at

https://doi.org/10.1021/acs.langmuir.2c02021
Langmuir 2022, 38, 12333−12345

2973, 2920, 2851, 1411, 1380, 1356, and 1164 cm^{-1} are attributed to the $\delta(CH_2)$ and $\delta(C-O)$ bending vibrations of D-glucuronic acid.[39] Similarly, the 1623 cm^{-1} peak of the hybrid nanomaterial SiO_2@GLA appears due to the $\nu(C=O)$ vibrations of the carboxyl groups of D-glucuronic acid. This is upshifted relative to D-glucuronic acid (1707 cm^{-1}) due to creating the pseudopeptide bond[39] between the surface amino groups and the carboxyl groups from GLA. This peptide-like linkage attributed the 1206 cm^{-1} peak to the C−N bond. Finally, the peaks at 455 ν(Si−OH) bend, 796 ν(Si−OH) stress, and 1093 cm^{-1} are the typical peaks for the ν(Si−O−Si) bonds (Figure S3(A) in the Supporting Information file).

In the FTIR spectra of SiO_2@GLAM in Figure 3 (orange line), the broad peak from 3347 to 3497 cm^{-1} is assigned to the OH groups of N-acetyl-D-glucosamine.[39] The peaks at 2962, 2932, 2909, 2886, and 2855 cm^{-1} are assigned to $\nu(CH_2)$, and those at 1501, 1461, 1431, 1416, and 1378 cm^{-1} are assigned to the $\delta(CH_2)$ groups. Also, the 1631 cm^{-1} peak due to the C=O vibrations of the carboxyl of N-acetyl-D-glucosamine is resolved in the spectrum of hybrid nanomaterial SiO_2@GLAM. Similarly, the 1550 cm^{-1} peak is assigned to NH-bond vibrations. Also, the peaks at 474 ν(Si−OH) bend, 801 ν(Si−OH) stress, and 1099 cm^{-1} are the typical peaks for the ν(Si−O−Si) bonds. Finally, N-acetyl-D-glucosamine's 1554 cm^{-1} peak of the N−H bond is resolved in Figure S3(B) in the Supporting Information file.

Finally, in Figure 3 (blue line), the FTIR spectrum of the doubly grafted hybrid {GLA@SiO_2@GLAM} [2:1] is presented. The 3385−3566 cm^{-1} peaks are assigned to OH groups, while the peaks at 2963, 2932, and 2849 cm^{-1} are attributed to $\nu(CH_2)$ vibrations; those at 1514, 1462, 1439, and 1416 cm^{-1} are attributed to the bending vibrations of the $\delta(CH_2)$ groups. The 1635 cm^{-1} peak of the bending vibrations of the C=O of the monomers is resolved. Interestingly, this is offset relative to each monomer, indicating that the GLA and GLAM may have some vibrational coupling. Furthermore, the peaks at 467 ν(Si−OH) bend, 800 ν(Si−OH) stress, and 1099 cm^{-1} are recognized as the typical peaks for the ν(Si−O−Si) bonds. Overall, the present FTIR data confirm the covalent bonding of both GLA and GLAM monomers on SiO_2 in the doubly grafted hybrid {GLA@SiO_2@GLAM} (Figure S3(C) in the Supporting Information file).

3.1.3.2. Raman Spectroscopy. In addition to FT-IR, Raman spectroscopy is a very sensitive technique utilized to primarily analyze the various structural components of the silica supporting nanomaterial, namely the internal siloxane configurations and the terminal surface silanol groups. Moreover, characteristic vibrations of the monosaccharides D-glucuronic acid and N-acetyl-D-glucosamine can be detected. Figure 4 depicts the Raman spectra of the monosaccharides D-glucuronic acid (GLA) (gray line) and N-acetyl-D-glucosamine (GLAM) (green line).

As shown in Figure 4, D-glucuronic acid (GLA) (gray line) and N-acetyl-D-glucosamine (green line) exhibit numerous peaks assigned to the different chemical bonds typical of monosaccharides. These include vibrations that originate from O−H and N−H functional groups as well as vibrations due to -COOH, $-CH_2$, $-NH_3^+$, and >N−H moieties.[40]

The characteristic peaks of the carbonyl moiety vibrations of D-glucuronic acid (GLA) (gray line) can be seen in 1074 cm^{-1} assigned to the ν(C−O) stretch, 1232 cm^{-1} assigned to ν(=C−O), 1365 cm^{-1} assigned to the δ(O−H) deformation, and 1708 cm^{-1} assigned to the ν(C=O) stretching vibration.[41]

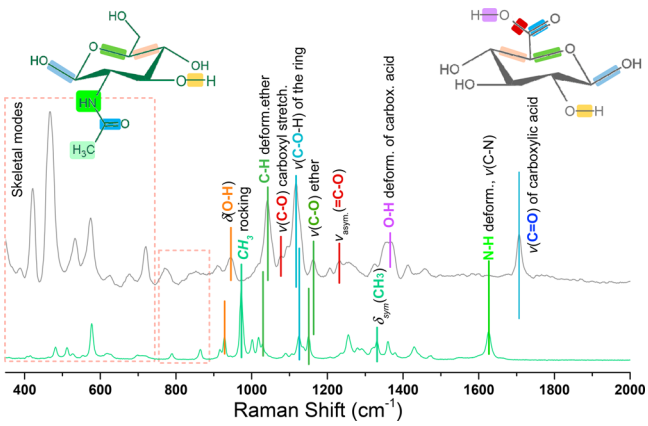

Figure 4. Raman analysis of the monosaccharides, the constituents of hyaluronic acid, D-glucuronic acid (gray line) and N-acetyl-D-glucosamine (green line).

GLA and GLAM present peaks assigned to the ring ether group vibrations. More specifically, the peaks at 1043 cm^{-1} (GLA) and 1029 cm^{-1} (GLAM) are assigned to the δ(C−H) deformation. Moreover, the peaks at 1118 cm^{-1} (GLA) and 1127 cm^{-1} (GLAM) are assigned to the ν(C−O−H) stretching, whereas the peaks at 1164 cm^{-1} (GLA) and 1149 cm^{-1} (GLAM) are assigned to the ν(C−O−C) stretching.[41] On the other hand, to cite just some of the characteristic bands of N-acetyl-D-glucosamine (green line), the band at ∼972 cm^{-1} is assigned to the rocking vibration of the CH_3 moiety, and 1626 cm^{-1} is assigned to the δ(N−H) deformation vibration.[41]

In contrast, Figure 5 presents the produced functionalized hybrid materials compared to their nonfunctionalized counterparts. The vibrations of silica are dominant in the spectra of the hybrid materials SiO_2@GLAM (panel A, dark green line), SiO_2@GLA (panel B, red line), and the doubly grafted nanohybrid {GLA@SiO_2@GLAM} [2:1] (panel C, orange line). The vibrations of the siloxane matrix, namely δ(Si−O−Si) *breathing modes*, are visible in the region of 300−600 cm^{-1}.[42] The band at ∼490 cm^{-1} is attributed to the typically formed 4-membered siloxane rings (4MRs).[42] Moreover, the presence of a broad peak below the 4MRs, namely in the region of 300−490 cm^{-1}, is assigned to higher-order siloxane rings such as 5-membered rings (5MRs), 6-membered rings (6MRs), etc.[42] This is in accordance with the TEM analysis since it confirms the stable and compact morphology of the supporting nanomaterial. Moreover, the silica matrix exhibits a characteristic band at ∼800 cm^{-1} assigned to the symmetric stretching vibration ν(Si−O−(Si)).[43]

Finally, in contrast to the unfunctionalized SiO_2 (see Figure 5(C) (blue line)), where the surface silanol groups exhibit a peak near ∼950 cm^{-1}, this peak is negligible in all the nanohybrid materials. The decrease of the peak intensity at ∼950 cm^{-1} in the hybrid materials confirms the successful grafting to the terminal surface silanols.

The disappearance of numerous peaks evident in the spectra of the initial monosaccharides, D-glucuronic acid and N-acetyl-D-glucosamine, can be attributed to the vibrational nature of this class of biomolecules, where stereochemistry plays a crucial role. The interaction of the incident light with the electric polarizability of the chemical bonds of the molecules directly depends on their specific configuration.[44]

Additionally, the Raman analysis indicates that the grafting procedures of the synthesis do not alter the siloxane matrix.

https://doi.org/10.1021/acs.langmuir.2c02021
Langmuir 2022, 38, 12333−12345

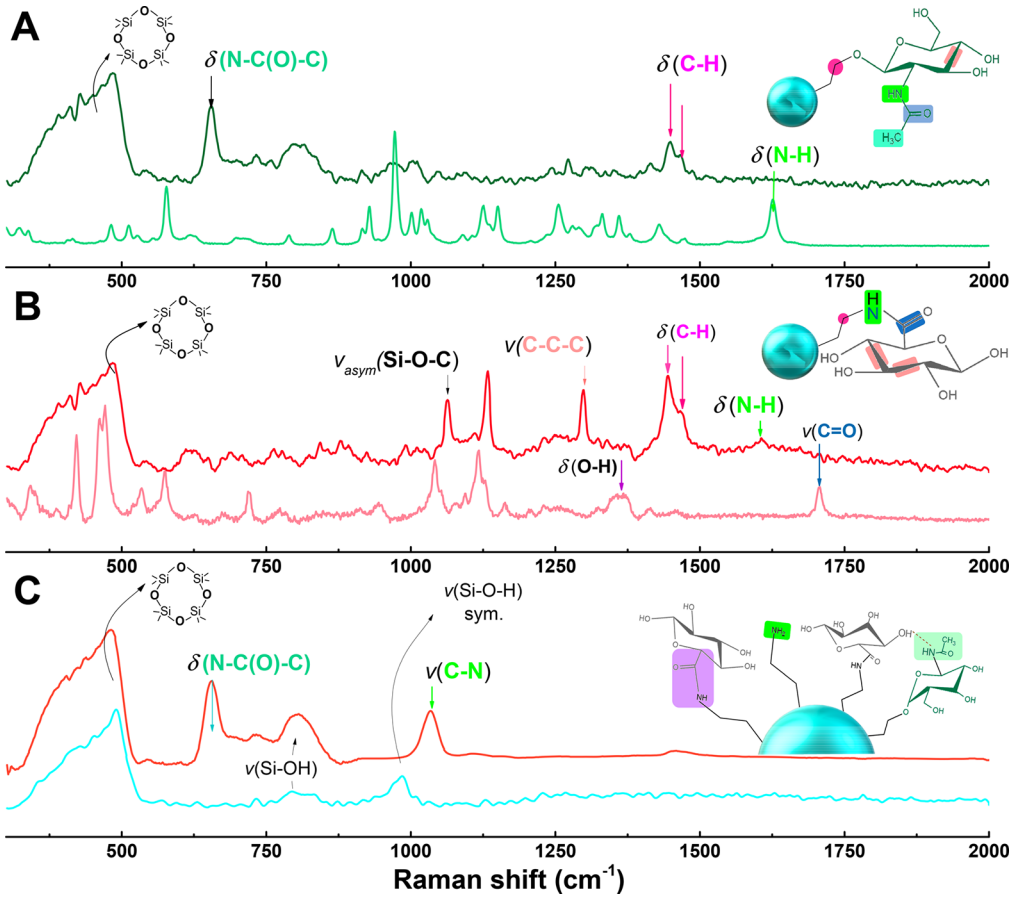

Figure 5. Raman spectra of (A) N-acetyl-D-glucosamine (GLAM) (light green line), SiO_2@GLAM (dark green line), (B) D-glucuronic acid (GLA) (pink line), SiO_2@GLA (red line), and (C) SiO_2 (blue line), and the doubly grafted nanohybrid {GLA@SiO_2@GLAM} [2:1] (orange line).

However, there is an obvious modification of the terminal silanol groups in all cases. Lastly, Raman analysis indicated the success of the functionalization since characteristic peaks are present, e.g., the pseudo-amide bond formation in the case of SiO_2@GLA at 1604 cm^{-1}.

3.2. Antioxidant Activity (Radical Scavenge Capacity) Evaluation. The solution of the DPPH radical has a characteristic purple color. Its absorbance at 515 nm can be utilized as a quantitative index; see calibration in Figure S4 in the Supporting Information file.[45,15,27] Addition of antioxidants results in quenching of the DPPH radicals, evidenced by a decrease of the peak intensity at 515 nm.[46−48] This DPPH-radical quenching is due to hydrogen-atom-transfer, where one H^+ and one electron e^- are transferred, i.e., as one hydrogen atom {H^+/e^-} from the -OH groups of the antioxidant to the DPPH radical.[17,27] As shown in a previous study by our group, gallic acid grafted on SiO_2 can successfully perform HAT to DPPH radicals[17,27] (see for comparison the kinetic curve for SiO_2@GA in Figure 6(B)). The present data, in Figure 6(A), show that SiO_2@GLA and {GLA@SiO_2@GLAM} hybrids are also able to perform hydrogen-atom-transfer to DPPH radical. In contrast, the SiO_2@GLAM nanohybrid is practically nonactive (Figure 6(A)).

Notably, the nongrafted GLA and GLAM and the simple mixture of SiO_2 with either GLA or GLAM are inactive; see Figures S5 and S6 and Scheme S5 in the Supporting Information file. See Section 3.2 for the experimental data in the Supporting Information file. The characteristic differences indicate that the grafting on the SiO_2 matrix exerts a profound beneficial effect on the HAT efficiency of GLA but not on the HAT activity of GLAM. More interestingly, the cografting of both GLA and GLAM appears to have a unique beneficial effect on their HAT efficiency toward DPPH radicals. There was, moreover, no loss of activity of the SiO_2@GLA and GLA@SiO_2@GLAM nanohybrids in powder form even after two years of being stored in the dark (see Figure S7 in the Supporting Information file).

As described earlier,[17] the kinetic profile of DPPH quenching provides vital information on the underlying radical-reaction events. In a semilogarithmic [$\ln(A{\cdot}A_o^{-1})$ vs t] plot, a single kinetic phase, eq 1, will become linear. Multiphase kinetics is manifested as a nonlinear [$\ln(A{\cdot}A_o^{-1})$ vs t] plot. In Figure 6(B), the initial fast-kinetic phase for SiO_2@GA is assigned to HAT,[17] while the kinetics at prolonged t > 150 s reflect complex radical−radical coupling events of gallic polyphenols.[17]

In Figure 6(C and D), the {GLA@SiO_2@GLAM} [2:1] and SiO_2@GLA hybrids show two distinct kinetic phases, labeled HAT_1 and HAT_ 2. The two-phase HAT is described by eq 2. The slopes of HAT_1 and HAT_2 are listed in Table 2. We underline that, in gallic acid, the secondary reactions are multiphase radical−radical couplings, not due to HAT.[17] These occur due to the high polymerization coupling activity of GA.[17,33] In the cases of GLA and GLAM, the molecules are not polyphenolics; that is, it is unlikely that they can perform radical polymerization. This has been verified herein by EPR spectroscopy, which shows zero radical formation by GLA of GLAM (data not shown). Thus, we consider that the two

https://doi.org/10.1021/acs.langmuir.2c02021
Langmuir 2022, 38, 12333−12345

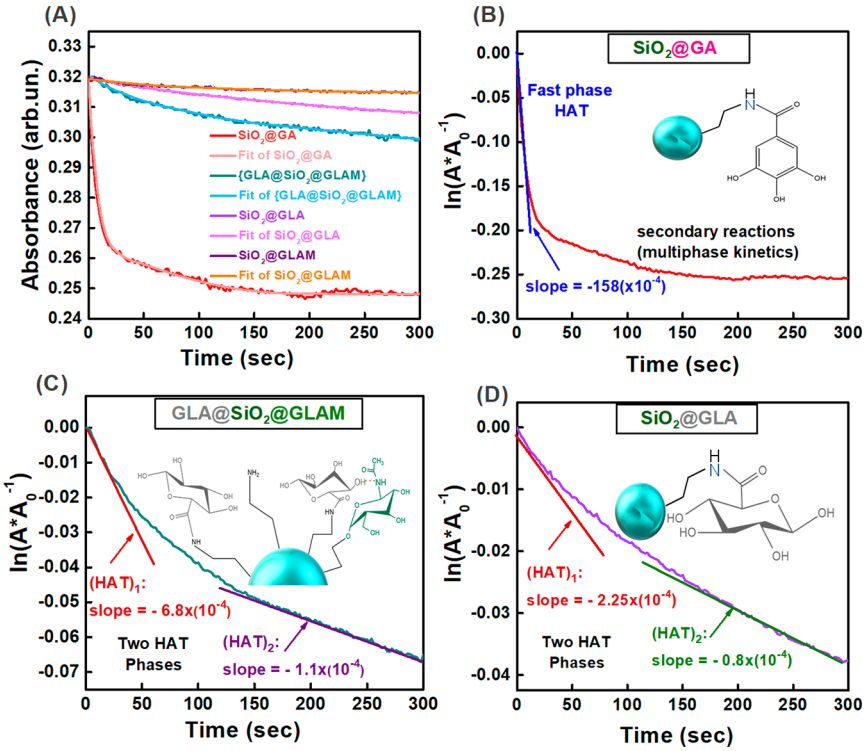

Figure 6. (A) Kinetics of decay of absorbance at 515 nm for DPPH radicals ($[DPPH]_0$ = 30.0 ± 0.1 μM) reacting with different nanohybrid materials, SiO_2@GA, SiO_2@GLA, SiO_2@GLAM, and doubly grafted {GLA@SiO_2@GLAM}. (B–D) Semilogarithmic [ln ($A{\cdot}A_o^{-1}$) vs t] plots of the data in (A). The two kinetic phases in (C) and (D) are attributed to two HAT activities in SiO_2@GLA and {GLA@SiO_2@GLAM}.

Table 2. DPPH Quenching Kinetic Rates by the SiO_2-Based Nanohybrid Materials

Material	*Kinetic Rates* ($\mu mol{\cdot}sec^{-1}$) × (10^{-4})
SiO_2@GA	*−158.0* ± 8
{GLA@SiO_2@GLAM} [2:1]	
HAT_1 phase	*−6.80* ± 0.3
HAT_2 phase	*−1.11* ± 0.05
SiO_2@GLA	
HAT 1_phase	*−2.25* ± 0.1
HAT 2_phase	*−0.08* ± 0.003
SiO_2@GLAM	
HAT_1 phase	∼−0.002 ± 0.0001
HAT_2 phase	*Not resolved*

kinetic phases in Figure 6(C and D) are due to HAT reactions. According to Table 2, HAT_2 has a similar rate, ca. -0.8×10^{-4} and -1.1×10^{-4}, in both materials. Intriguingly, the fast phase, HAT_1, in {GLA@SiO_2@GLAM} has a significantly faster rate, -6.8×10^{-4} vs -2.25×10^{-4}, in SiO_2@GLA.

Overall, the kinetics in Figure 6 and Table 2 reveal that the HAT rate follows the order:

$$\textbf{\textit{SiO}}_2\textbf{\textit{@GA}} \gg \{\textbf{\textit{GLA@SiO}}_2\textbf{\textit{@GLAM}}\} > \{\textbf{\textit{SiO}}_2\textbf{\textit{@GLA}}\} \gg \{\textbf{\textit{SiO}}_2\textbf{\textit{@GLAM}}\} \sim \mathbf{0}$$

The above order indicates that the doubly grafted nanohybrid {GLA@SiO_2@GLAM} [2:1] has a 30% faster HAT_1 kinetic than SiO_2@GLA. Taking into account the poor performance of SiO_2@GLAM, see Table 2, this is rather unexpected; if we would assume a simple additive performance of the two components SiO_2@GLA and SiO_2@GLAM in the doubly grafted {GLA@SiO_2@GLAM} [2:1], then the rate of {GLA@SiO_2@GLAM} should be the average of SiO_2@GLA and SiO_2@GLAM, which is not the case. Table 2 reveals that the doubly grafted system {GLA@SiO_2@GLAM} [2:1] has improved HAT_1 performance, indicating that a beneficial interaction between the two components GLA and GLAM occurs when both are on the same particle. There is ample literature evidence that the critical parameter which determines the HAT efficiency in these systems is the O–H bond-dissociation-enthalpy (BDE),[49−51,45] which determines the activation energy barrier (E_a) of the HAT process. Hereafter, to better understand the fundamentals for this phenomenon, a detailed kinetic Arrhenius study has been carried out to obtain a numerical estimate of E_a of the HAT efficiency, with specific emphasis on the best performing, doubly grafted {GLA@SiO_2@GLAM} hybrid.

3.2.1. Temperature-Dependent Arrhenius-Kinetics Analysis. The DPPH scavenging kinetic profiles for the SiO_2@GLA are presented in Figure 7(A and B), respectively, for reaction temperatures in the range of −15 °C to +25 °C.

For the analysis of the kinetic traces, we use the two kinetic rates, HAT_1 and HAT_2, obtained from the [$\ln(A{\cdot}A_o^{-1})$ vs t] plot as shown in graphs (C and D). In this way, we derive two values of activation energies, E_a, for the two HAT processes for each material, listed in Table 3. We have additionally derived the number of scavenged DPPH radicals per active molecule in Table 3.[17] In brief, for every experiment, the amount of DPPH radicals quenched via the HAT process, N_{DPPH}, has been estimated. Then, by dividing N_{DPPH} by the total number, N_{total}, of GLA or GLAM molecules present in each sample, we obtain stoichiometry ratios n_{HAT}, i.e., the number of hydrogen-atom-transfer efficiency (eq 3). For the kinetic analysis of the doubly grafted {GLA@SiO_2@GLAM} [3:1], see Figure S8 in the Supporting Inform file.

https://doi.org/10.1021/acs.langmuir.2c02021
Langmuir 2022, 38, 12333−12345

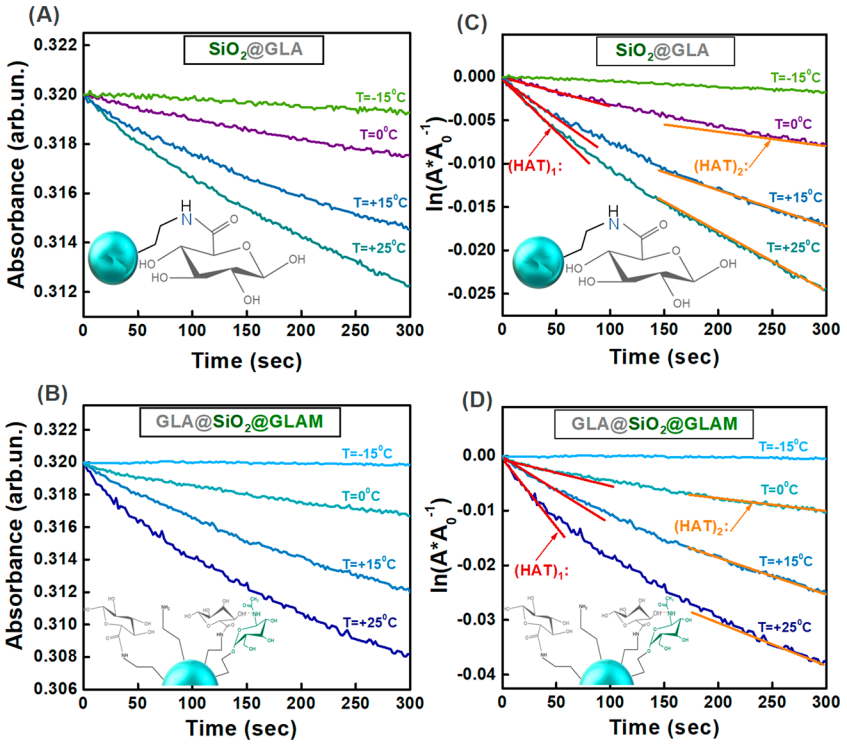

Figure 7. DPPH radical quenching, monitored via the 515 nm absorbance of DPPH radical, at the different temperatures +25 °C, +15 °C, 0 °C, and −15 °C for SiO_2@GLA (A, C) and {GLA@SiO_2@GLAM} [2:1] (B, D). Panels (C, D) are the semilogarithmic [ln ($A{\cdot}A_o^{-1}$) vs t] plots of the data in (A, B), respectively. The arrows mark the two HAT_1 and HAT_2 phases.

Table 3. HAT Stoichiometry Ratios n_{HAT} and Activation Energies E_a for the Present Nanohybrids

Material	n_{HAT} (±0.2)	E_a (kJ/mol (±1))
SiO_2@GA	2.0	34.0[17]
Gallic Acid	1.6	42.2[17]
{GLA@SiO_2@GLAM} [2:1][a]	1.1	HAT_1 42.2
		HAT_2 55.5
{GLA@SiO_2@GLAM} [3:1][a]	1.1	HAT_1 46.6
		HAT_2 61.5
SiO_2@GLA	1.1	HAT_1 65.7
		HAT_2 76.2
SiO_2@GLAM	0.2	HAT_1 123.3

[a]The molar ratio [3:1] or [2:1] refers to [GLA:GLAM] grafted molecules on SiO_2 based on TGA data.

$$n_{HAT} = N_{DPPH}/N_{total} \quad (3)$$

3.2.1.1. HAT Stoichiometry. The HAT stoichiometry has been calculated only for the total DPPH quenching process to simplify the analysis. The n_{HAT} values in Table 3 show that the doubly grafted nanohybrid {GLA@SiO_2@GLAM} and monografted SiO_2@GLA achieve $n_{fast} \sim 1$ while the monografted SiO_2@GLAM achieved much lower $n_{HAT} \sim 0.2$, respectively. This finding indicates that, in the doubly grafted nanohybrid {GLA@SiO_2@GLAM}, a highly active OH group donates one hydrogen atom to nearby DPPH radicals. Compared with the SiO_2@GLA or SiO_2@GLAM, we infer that in the doubly grafted nanohybrid {GLA@SiO_2@GLAM} practically, the SiO_2@GLA adduct determines the HAT activity. Overall, the present n_{HAT} data reveal that

[i] only the grafted GLA moiety has the electronic configuration to allow a considerable HAT process to a DPPH radical,

[ii] grafting of GLA on SiO_2 facilitates the kinetic rate of HAT; however, the n_{HAT} does not change, i.e., it remains ∼1. This indicates that a single OH unit in GLA is active in HAT, which could be the free C1-OH group of the GLA molecule, according to the DFT study of Taylor et al.[52] Grafting on SiO_2 accelerates the HAT rates. This is due to a lowering of E_a (see Figure 8). The beneficial effect of grafting on SiO_2 has been initially observed for gallic acid[17] and attributed to a lowering of the activation energy of the process, and

[iii] cografting of GLA and GLAM on the same SiO_2 particle promotes the HAT rates decisively. However, the n_{HAT} does not change, i.e., it remains ∼1. This indicates a single OH unit in {GLA@SiO_2@GLAM} which is active in HAT. This is the moiety belonging to GLA and probably is the same C1-OH unit responsible for the HAT activity of SiO_2@GLA and which is still available in {GLA@SiO_2@GLAM}.

3.2.1.2. Activation Energies (E_a). Figure 8 presents a bar graph of the E_a values from Table 3. The E_a values reveal that

[i] compared to SiO_2@GA, all the present SiO_2@GLAM, SiO_2@GLA, and {GLA@SiO_2@GLAM} hybrids have higher E_a barriers. The low E_a value for GA and SiO_2@GA is the reason for Gallic acid's well-established superior antioxidant activity.[17] The E_a of SiO_2@GALM is 123 k J mol^{-1}, which is relatively high, which determines its lack of activity as a HAT antioxidant,

[ii] the two HAT phases in SiO_2@GLA have considerably different E_a values: the slow HAT_2 phase is limited by a 10 kJ·mol^{-1} higher activation barrier vs the faster HAT_1 phase, and

[iii] the doubly grafted {GLA@SiO_2@GLAM} is characterized by a considerably lower E_a, i.e., by 21−24 kJ·

https://doi.org/10.1021/acs.langmuir.2c02021
Langmuir 2022, 38, 12333−12345

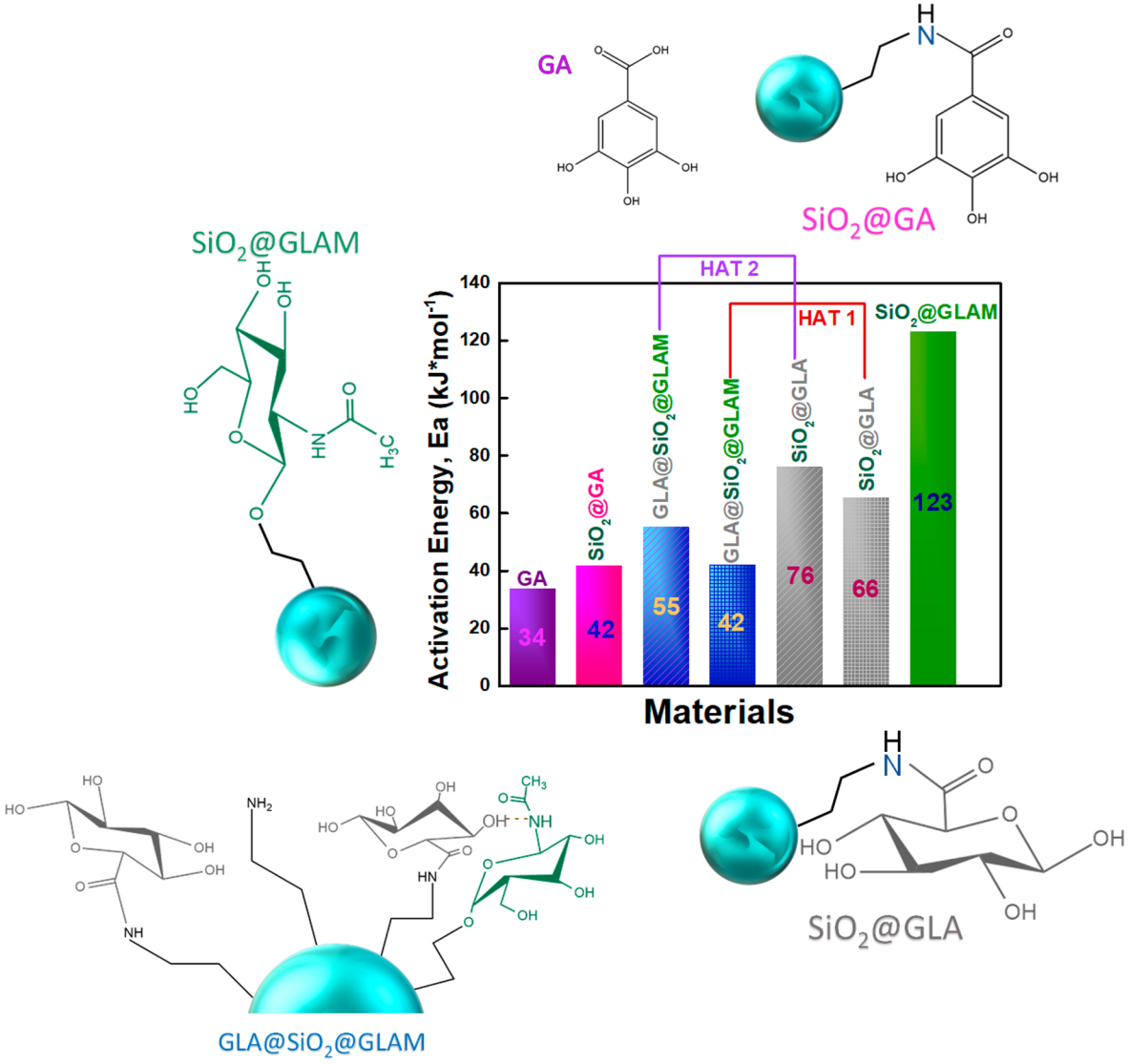

Figure 8. Activation energy barriers for the present SiO_2-based nanohybrid materials. The E_a values for the two HAT phases (HAT_1, HAT_2) in SiO_2@GLA and {GLA@SiO_2@GLAM} are marked.

mol^{-1}, vs the SiO_2@GLA. Thus, the doubly grafted {GLA@SiO_2@GLAM} nanohybrid has a thermodynamically favorable configuration that promotes the transfer of hydrogen atoms to DPPH radicals.

According to Foti et al.[9,10,53] and our work,[17,18] the key factors that influence the activation energy E_a of the hydrogen-atom-transfer (HAT) process by various phenolic molecules to the DPPH radical include local H-bonding phenomena of the OH groups, solvent polarity/local dipoles, and steric effects. Herein, the GLA or GLAM molecules are not phenolics. However, the present data indicate that a common mechanism should be operative in SiO_2-grafted nanohybrids. The SiO_2 matrix is lowering the E_a values in all cases. We consider that local H-bonding between the OH moiety of GLA and the SiO_2 is crucial in this process. In addition, the coexistence of GLAM exerts a further beneficial role on GLA. In this context, the two HAT phases detected in GLA nanohybrids can correspond to two different local H-bonding environments of GLA on the SiO_2 matrix (see Figure 9).

4. CONCLUSIONS

Hyaluronic acid components can be active antioxidants when properly grafted on the SiO_2 surface. This opens new perspectives not foreseen so far. The two building blocks of hyaluronic acid, D-glucuronic acid (GLA) and N-acetyl-D-glucosamine (GLAM), have been covalently grafted on SiO_2 nanoparticles. All SiO_2-based nanohybrids show enhanced antioxidant activity, while nongrafted GLA and GLAM are inactive antioxidants. SiO_2@GLAM was inactive. The doubly grafted {GLA@SiO_2@GLAM} nanohybrid shows significantly enhanced antioxidant activity vs the single-component SiO_2@GLA. The antioxidant mechanism is based on hydrogen-atom-transfer (HAT) from a single OH group of GLA to DPPH. Two HAT phases, fast and slow, are consistently resolved in {GLA@SiO_2@GLAM} and SiO_2@GLA. The Arrhenius study shows that the activation energy barrier for the fast HAT_1 process is E_a = 42 kJ·mol^{-1}; that for the doubly grafted {GLA@SiO_2@GLAM} is significantly lower, by 24 kJ·mol^{-1}, vs E_a of the single-component SiO_2@GLA hybrid. A synergy between the OH groups of surface-grafted GLA/GLAM moieties is suggested to be the basis of the lower E_a observed

https://doi.org/10.1021/acs.langmuir.2c02021
Langmuir 2022, 38, 12333−12345

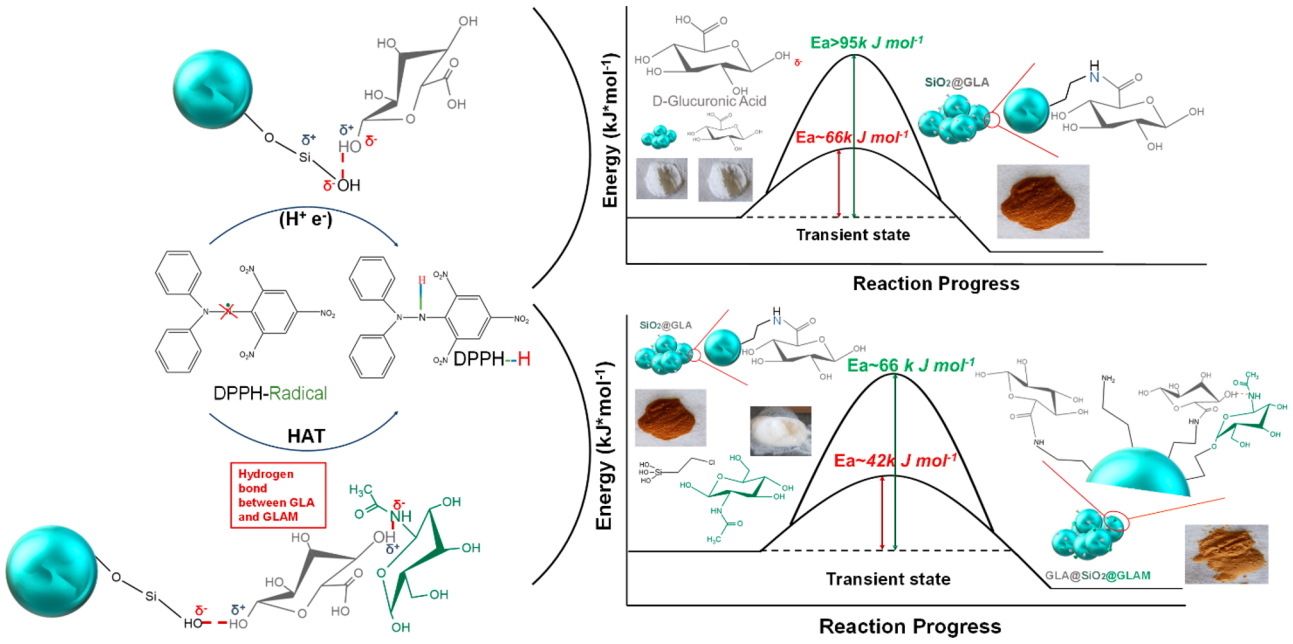

Figure 9. Proposed thermodynamic process of hydrogen atom transfer: (*left*) the local H-bonding facilitates the automatic transfer of one H^+ and one e^- from the OH group of GLA to the DPPH radical; (*right*) the beneficial effect of the local H-bonding network causes a significant drop in the energy activation barrier.

for the doubly grafted {GLA@SiO_2@GLAM} hybrid. The present study reveals that hybrid materials allow thermodynamic processes that are not favored in their single-component counterparts. Thus, the present work introduces a novel concept for engineering new antioxidant platforms and permits basic research that enables the tuning of materials properties toward—so far unpreviewed—applications interfaced with health and biomedical problems.

■ ASSOCIATED CONTENT

Supporting Information

The Supporting Information is available free of charge at https://pubs.acs.org/doi/10.1021/acs.langmuir.2c02021.

Scheme S1. Process for the synthesis of SiO_2@GLA. Scheme S2. Process for the synthesis of SiO_2@GLAM. Scheme S3. Process for the synthesis of the doubly grafted {GLA@SiO_2@GLAM} [2:1]. Section 2.4. Preparation of the doubly grafted {GLA@SiO_2@GLAM} [3:1]. Scheme S4. Process for the synthesis of the doubly grafted {GLA@SiO_2@GLAM} [3:1]. Figure S1. N_2-sorption isotherms and pore-size analysis (BET) analysis for the materials. Section 3.1.2. Thermogravimetric analysis. Figure S2. Thermographs of the materials. Figure S3. FT-IR spectra of the materials. Figure S4. Calibration curves for the DPPH molecule in a solution of MeOH. Figure S5. Illustration of the kinetic curves of D-glucuronic acid and N-acetyl-D-glucosamine. Section 3.2. Antioxidant activity (radical scavenging capacity) evaluation. Figure S6. Kinetics of decay of absorbance at 515 nm for DPPH with the monomers. Scheme S5. Schematic representation of the adsorption of monomers on the silica surface. Figure S7. (A) Functionalized SiO_2@GLA, (B) functionalized SiO_2@GLAM, and (C) functionalized {GLA@SiO_2@GLAM}. Figure S8. DPPH radical quenching monitored via the 515 nm absorbance of DPPH radical at different temperatures (PDF)

■ AUTHOR INFORMATION

Corresponding Author

Maria Louloudi − *Laboratory of Biomimetic Catalysis & Hybrid Materials, Department of Chemistry, University of Ioannina, GR-45110 Panepistimioupoli Ioannina, Greece*; Email: mlouloud@uoi.gr

Authors

Annita Theofanous − *Laboratory of Biomimetic Catalysis & Hybrid Materials, Department of Chemistry, University of Ioannina, GR-45110 Panepistimioupoli Ioannina, Greece*; orcid.org/0000-0002-8396-8257

Irene Sarli − *Laboratory of Biomimetic Catalysis & Hybrid Materials, Department of Chemistry, University of Ioannina, GR-45110 Panepistimioupoli Ioannina, Greece*

Fotini Fragou − *Laboratory of Biomimetic Catalysis & Hybrid Materials, Department of Chemistry, University of Ioannina, GR-45110 Panepistimioupoli Ioannina, Greece*; orcid.org/0000-0001-5302-3159

Eleni Bletsa − *Laboratory of Physical Chemistry of Materials & Environment, Department of Physics, University of Ioannina, GR-45110 Panepistimioupoli Ioannina, Greece*

Yiannis Deligiannakis − *Laboratory of Physical Chemistry of Materials & Environment, Department of Physics, University of Ioannina, GR-45110 Panepistimioupoli Ioannina, Greece*; orcid.org/0000-0002-9390-4222

Complete contact information is available at: https://pubs.acs.org/10.1021/acs.langmuir.2c02021

Author Contributions

AT performed the experiments, data analysis, sample preparation, and manuscript writing. *IS* contributed to sample preparation. *FF* performed Raman spectroscopy and data

https://doi.org/10.1021/acs.langmuir.2c02021
Langmuir 2022, 38, 12333−12345

analysis. *EB* worked on data analysis. *YD* performed project conceptualization, theoretical analysis, and manuscript writing. *ML* performed project conceptualization, data analysis, design of experiments, and manuscript writing.

Notes

The authors declare no competing financial interest.

■ ACKNOWLEDGMENTS

This work has been supported by the project "Center For Research, Quality Analysis Of Cultural Heritage Materials and Communication Of Science" (MIS 5047233) implemented under the Action "Reinforcement of the Research and Innovation Infrastructure", funded by the Operational Program "Competitiveness, Entrepreneurship and Innovation" (NSRF 2014-2020) and cofinanced by Greece and the European Union (European Regional Development Fund).

■ ABBREVIATIONS

GLA, D-glucuronic acid,; GLAM, N-acetyl-D-glucosamine; HyA, hyaluronic acid; HAT, hydrogen-atom-transfer; GA, gallic acid; RSC, radicals scavenging capacity

■ REFERENCES

(1) Khalil, I.; Yehye, W. A.; Etxeberria, A. E.; Alhadi, A. A.; Dezfooli, S. M.; Julkapli, N. B. M.; Basirun, W. J.; Seyfoddin, A. Nanoantioxidants: Recent Trends in Antioxidant Delivery Applications. *Antioxidants* **2020**, *9* (1), 24.

(2) Omran, B.; Baek, K.-H. Nanoantioxidants: Pioneer Types, Advantages, Limitations, and Future Insights. *Molecules* **2021**, *26* (22), 7031.

(3) Tułodziecka, A.; Szydłowska-Czerniak, A. Determination of Total Antioxidant Capacity of Rapeseed and Its By-Products by a Novel Cerium Oxide Nanoparticle-Based Spectrophotometric Method. *Food Anal. Methods* **2016**, *9* (11), 3053−3062.

(4) Dubé, N.; A.-M., S.; Laroche, G.; V, P. Additives in Biomedical Polyurethanes. *Biomedical Applications of Polyurethanes* **2001**, *6*, 55−76.

(5) Halliwell, B. Antioxidants in Human Health and Disease. *Annu. Rev. Nutr.* **1996**, *16* (1), 33−50.

(6) Aruoma, O. I. Free Radicals, Oxidative Stress, and Antioxidants in Human Health and Disease. *J. Amer Oil Chem. Soc.* **1998**, *75* (2), 199−212.

(7) Balasundram, N.; Sundram, K.; Samman, S. Phenolic Compounds in Plants and Agri-Industrial by-Products: Antioxidant Activity, Occurrence, and Potential Uses. *Food Chem.* **2006**, *99* (1), 191−203.

(8) Foti, M. C. Antioxidant Properties of Phenols. *J. Pharm. Pharmacol.* **2010**, *59* (12), 1673−1685.

(9) Foti, M. C.; Amorati, R.; Pedulli, G. F.; Daquino, C.; Pratt, D. A.; Ingold, K. U. Influence of "Remote" Intramolecular Hydrogen Bonds on the Stabilities of Phenoxyl Radicals and Benzyl Cations. *J. Org. Chem.* **2010**, *75* (13), 4434−4440.

(10) Foti, M. C.; Daquino, C. Kinetic and Thermodynamic Parameters for the Equilibrium Reactions of Phenols with the Dpph? Radical. *Chem. Commun.* **2006**, No. 30, 3252.

(11) Rice-Evans, C.; Miller, N.; Paganga, G. Antioxidant Properties of Phenolic Compounds. *Trends in Plant Science* **1997**, *2* (4), 152−159.

(12) Stratil, P.; Klejdus, B.; Kubáň, V. Determination of Total Content of Phenolic Compounds and Their Antioxidant Activity in VegetablesEvaluation of Spectrophotometric Methods. *J. Agric. Food Chem.* **2006**, *54* (3), 607−616.

(13) Blois, M. S. Antioxidant Determinations by the Use of a Stable Free Radical. *Nature* **1958**, *181* (4617), 1199−1200.

(14) Bondet, V.; Brand-Williams, W.; Berset, C. Kinetics and Mechanisms of Antioxidant Activity Using the DPPH.Free Radical Method. *LWT - Food Science and Technology* **1997**, *30* (6), 609−615.

(15) Brand-Williams, W.; Cuvelier, M. E.; Berset, C. Use of a Free Radical Method to Evaluate Antioxidant Activity. *LWT - Food Science and Technology* **1995**, *28* (1), 25−30.

(16) Foti, M. C. Use and Abuse of the DPPH • Radical. *J. Agric. Food Chem.* **2015**, *63* (40), 8765−8776.

(17) Deligiannakis, Y.; Sotiriou, G. A.; Pratsinis, S. E. Antioxidant and Antiradical SiO_2 Nanoparticles Covalently Functionalized with Gallic Acid. *ACS Appl. Mater. Interfaces* **2012**, *4* (12), 6609−6617.

(18) Sotiriou, G. A.; Blattmann, C. O.; Deligiannakis, Y. Nano-antioxidant-Driven Plasmon Enhanced Proton-Coupled Electron Transfer. *Nanoscale* **2016**, *8* (2), 796−803.

(19) Bletsa, E.; Stathi, P.; Dimos, K.; Louloudi, M.; Deligiannakis, Y. Interfacial Hydrogen Atom Transfer by Nanohybrids Based on Humic Acid Like Polycondensates. *J. Colloid Interface Sci.* **2015**, *455*, 163−171.

(20) Cai, J.; Fu, J.; Li, R.; Zhang, F.; Ling, G.; Zhang, P. A Potential Carrier for Anti-Tumor Targeted Delivery-Hyaluronic Acid Nanoparticles. *Carbohydr. Polym.* **2019**, *208*, 356−364.

(21) Ashrafizadeh, M.; Mirzaei, S.; Gholami, M. H.; Hashemi, F.; Zabolian, A.; Raei, M.; Hushmandi, K.; Zarrabi, A.; Voelcker, N. H.; Aref, A. R.; Hamblin, M. R.; Varma, R. S.; Samarghandian, S.; Arostegi, I. J.; Alzola, M.; Kumar, A. P.; Thakur, V. K.; Nabavi, N.; Makvandi, P.; Tay, F. R.; Orive, G. Hyaluronic Acid-Based Nanoplatforms for Doxorubicin: A Review of Stimuli-Responsive Carriers, Co-Delivery and Resistance Suppression. *Carbohydr. Polym.* **2021**, *272*, 118491.

(22) Kim, H.; Jeong, H.; Han, S.; Beack, S.; Hwang, B. W.; Shin, M.; Oh, S. S.; Hahn, S. K. Hyaluronate and Its Derivatives for Customized Biomedical Applications. *Biomaterials* **2017**, *123*, 155−171.

(23) Zhai, P.; Peng, X.; Li, B.; Liu, Y.; Sun, H.; Li, X. The Application of Hyaluronic Acid in Bone Regeneration. *Int. J. Biol. Macromol.* **2020**, *151*, 1224−1239.

(24) Chen, W. Y. J. Functions of Hyaluronan in Wound Repair. *Hyaluronan*; Elsevier, 2002; pp 147−156. DOI: 10.1533/9781845693121.147.

(25) Pasanphan, W.; Buettner, G. R.; Chirachanchai, S. Chitosan Conjugated with Deoxycholic Acid and Gallic Acid: A Novel Biopolymer-Based Additive Antioxidant for Polyethylene. *J. Appl. Polym. Sci.* **2008**, *109* (1), 38−46.

(26) Cho, Y.-S.; Kim, S.-K.; Ahn, C.-B.; Je, J.-Y. Preparation, Characterization, and Antioxidant Properties of Gallic Acid-Grafted-Chitosans. *Carbohydr. Polym.* **2011**, *83* (4), 1617−1622.

(27) Mishra, K.; Ojha, H.; Chaudhury, N. K. Estimation of Antiradical Properties of Antioxidants Using DPPH Assay: A Critical Review and Results. *Food Chem.* **2012**, *130* (4), 1036−1043.

(28) Cirillo, G.; Kraemer, K.; Fuessel, S.; Puoci, F.; Curcio, M.; Spizzirri, U. G.; Altimari, I.; Iemma, F. Biological Activity of a Gallic Acid-Gelatin Conjugate. *Biomacromolecules* **2010**, *11* (12), 3309−3315.

(29) Aytekin, A. O.; Morimura, S.; Kida, K. Synthesis of Chitosan-Caffeic Acid Derivatives and Evaluation of Their Antioxidant Activities. *J. Biosci. Bioeng.* **2011**, *111* (2), 212−216.

(30) Arrua, D.; Strumia, M. C.; Nazareno, M. A. Immobilization of Caffeic Acid on a Polypropylene Film: Synthesis and Antioxidant Properties. *J. Agric. Food Chem.* **2010**, *58* (16), 9228−9234.

(31) Gournis, D.; Deligiannakis, Y.; Karakassides, M. A.; Boussac, A.; Ioannidis, N.; Petridis, D. Stability Study of Tyrosinate Radical in a Restricted Phyllomorphous Medium. *Langmuir* **2002**, *18* (25), 10024−10029.

(32) Giannakopoulos, E.; Stathi, P.; Dimos, K.; Gournis, D.; Sanakis, Y.; Deligiannakis, Y. Adsorption and Radical Stabilization of Humic-Acid Analogues and Pb^{2+} on Restricted Phyllomorphous Clay. *Langmuir* **2006**, *22* (16), 6863−6873.

(33) Panagiota, S.; Louloudi, M.; Deligiannakis, Y. EPR Study of Phenolic Radical Stabilization by Grafting on SiO2. *Chem. Phys. Lett.* **2009**, *472* (1−3), 85−89.

(34) Technical University of Lodz, Institute of Polymer and Dye Technology, Faculty of Chemistry, 90-924 Lodz, ul. Stefanowskiego 12/16, Poland; Masek, A. Antioxidant Potential of Hydroxycinnamic Acids in Advanced Oxidation Processes. *Int. J. Electrochem. Sci.* **2016**, 8848−8860. DOI: 10.20964/2016.10.12.
(35) Luo, C.-L.; Zhou, Q.; Yang, Z.-W.; Wang, R.-D.; Zhang, J.-L. Evaluation of Structure and Bioprotective Activity of Key High Molecular Weight Acylated Anthocyanin Compounds Isolated from the Purple Sweet Potato (Ipomoea Batatas L. Cultivar Eshu No.8). *Food Chem.* **2018**, *241*, 23−31.
(36) Logan, S. R. The Origin and Status of the Arrhenius Equation. Journal of Chemical Education. *J. Chem. Educ.* **1982**, *59* (4), 279.
(37) Bates, J. B. Fourier Transform Infrared Spectroscopy. *Science* **1976**, *191* (4222), 31−37.
(38) Hunger, M. W. J. In Situ IR, NMR, EPR, and UV/Vis Spectroscopy: Tools for New Insight into the Mechanisms of Heterogeneous Catalysis. *Angewandte Chemie International Edition* **2001**, *40* (16), 2954−2971.
(39) Kovács, A.; Nyerges, B.; Izvekov, V. Vibrational Analysis of *N* -Acetyl-α- D -Glucosamine and β- D -Glucuronic Acid. *J. Phys. Chem. B* **2008**, *112* (18), 5728−5735.
(40) She, C. Y.; Dinh, N. D.; Tu, A. T. Laser Raman Scattering of Glucosamine N-Acetylglucosamine, and Glucuronic Acid. *Biochimica et Biophysica Acta (BBA) - General Subjects* **1974**, *372* (2), 345−357.
(41) Socrates, G. *Infrared and Raman Characteristic Group Frequencies: Tables and Charts*, 3rd ed., repr. as paperback; Wiley: Chichester, 2010.
(42) Zhang, H.; Dunphy, D. R.; Jiang, X.; Meng, H.; Sun, B.; Tarn, D.; Xue, M.; Wang, X.; Lin, S.; Ji, Z.; Li, R.; Garcia, F. L.; Yang, J.; Kirk, M. L.; Xia, T.; Zink, J. I.; Nel, A.; Brinker, C. J. Processing Pathway Dependence of Amorphous Silica Nanoparticle Toxicity: Colloidal vs Pyrolytic. *J. Am. Chem. Soc.* **2012**, *134* (38), 15790−15804.
(43) Capeletti, L. B.; Baibich, I. M.; Butler, I. S.; dos Santos, J. H. Z. Infrared and Raman Spectroscopic Characterization of Some Organic Substituted Hybrid Silicas. *Spectrochimica Acta Part A: Molecular and Biomolecular Spectroscopy* **2014**, *133*, 619−625.
(44) Mutter, S. T.; Zielinski, F.; Cheeseman, J. R.; Johannessen, C.; Popelier, P. L. A.; Blanch, E. W. Conformational Dynamics of Carbohydrates: Raman Optical Activity of D -Glucuronic Acid and N-Acetyl- D -Glucosamine Using a Combined Molecular Dynamics and Quantum Chemical Approach. *Phys. Chem. Chem. Phys.* **2015**, *17* (8), 6016−6027.
(45) Pratsinis, S. E. History of Manufacture of Fine Particles in High-Temperature Aerosol Reactors. *Aerosol science and technology: History and reviews*; RTI International: USA, 2011; pp 475−507.
(46) Alam, Md. N.; Bristi, N. J.; Rafiquzzaman, Md. Review on in Vivo and in Vitro Methods Evaluation of Antioxidant Activity. *Saudi Pharmaceutical Journal* **2013**, *21* (2), 143−152.
(47) Tailor, C. S.; Goyal, A. Antioxidant Activity by DPPH Radical Scavenging Method of Ageratum conyzoides Linn. Leaves. *American Journal of Ethnomedicine* **2014**, *1* (4), 244−249.
(48) Hammes-Schiffer, S. Comparison of Hydride, Hydrogen Atom, and Proton-Coupled Electron Transfer Reactions. *ChemPhysChem* **2002**, *3* (1), 33−42.
(49) Košinová, P.; Di Meo, F.; Anouar, E. H.; Duroux, J.-L.; Trouillas, P. H-Atom Acceptor Capacity of Free Radicals Used in Antioxidant Measurements: H-Atom Acceptor in Antioxidant Measurements. *Int. J. Quantum Chem.* **2011**, *111* (6), 1131−1142.
(50) Wright, J. S.; Johnson, E. R.; DiLabio, G. A. Predicting the Activity of Phenolic Antioxidants: Theoretical Method, Analysis of Substituent Effects, and Application to Major Families of Antioxidants. *J. Am. Chem. Soc.* **2001**, *123* (6), 1173−1183.
(51) Evans, M. G.; Polanyi, M. Further Considerations on the Thermodynamics of Chemical Equilibria and Reaction Rates. *Trans. Faraday Soc.* **1936**, *32*, 1333.
(52) Turner, J. A.; Adrianov, T.; Zakaria, M. A.; Taylor, M. S. Effects of Configuration and Substitution on C-H Bond Dissociation Enthalpies in Carbohydrate Derivatives: A Systematic Computational Study. *J. Org. Chem.* **2022**, *87* (2), 1421−1433.
(53) Foti, M. C.; Daquino, C.; Mackie, I. D.; DiLabio, G. A.; Ingold, K. U. Reaction of Phenols with the 2,2-Diphenyl-1-Picrylhydrazyl Radical. Kinetics and DFT Calculations Applied To Determine ArO-H Bond Dissociation Enthalpies and Reaction Mechanism. *J. Org. Chem.* **2008**, *73* (23), 9270−9282.